ELEVENTH EUROPEAN ROTORCRAFT FORUM

Paper No. 28

ANALYSIS OF THE WAKE DYNAMICS OF A TYPICAL TILT-ROTOR CONFIGURATION IN TRANSITION FLIGHT

David R. Clark
Analytical Methods, Inc.
Redmond, Washington, U.S.A.

and

Michael A. McVeigh
Bell-Boeing
Philadelphia, Pennsylvania, U.S.A.

September 10-13, 1985

London, England.

THE CITY UNIVERSITY, LONDON, EC1V OHB, ENGLAND.

ANALYSIS OF THE WAKE DYNAMICS OF A TYPICAL TILT-ROTOR CONFIGURATION IN TRANSITION FLIGHT

David R. Clark
Analytical Methods, Inc.
Redmond, Washington, U.S.A.

Michael A. McVeigh
Bell-Boeing
Philadelphia, Pennsylvania U.S.A.

Abstract

The paper presents the results of an analytical study of the wake dynamics of a tilt-rotor wind tunnel model in transition flight. As a prelude to the analysis of the tilt-rotor configuration and in order to build confidence in the computer program it was used in a study of a simple tilt-propeller/wing combination tested by NASA. Correlation of calculated forces and moments throughout the transition speed range was excellent.

Based upon the success of the preliminary study, a panel model of an early wind tunnel model of the V-22 tilt-rotor aircraft was developed. The characteristics of this configuration were explored for a wide range of conditions in the helicopter mode, from hover into forward flight, and the interaction between rotor and wing wakes investigated in detail. The paper presents examples of this interaction, and discusses the effect of rotor-induced changes in wing loading as a function of air speed at representative flight conditions.

Introduction

The tilt-rotor aircraft combines in one configuration the hover/low speed capabilities of a helicopter with the high-speed/high altitude/long range flight capability of a fixed-wing aircraft. With the success of the XV-15 development, a substantial wind tunnel and flight data base has now been accumulated on this configuration. This experience is being applied to the development of the V-22 multi-mission tilt-rotor. However, gaps still exist in our knowledge of fundamental flowfield effects on the tilt-rotor configuration. In particular, the precise interactions between the two rotors in the system and between the rotors and the wing are not easily

investigated in a wind tunnel test where only integrated forces and moments and some surface pressure data are available. Details on the flowfield development are obtainable in a wind tunnel test only at great expense with time-consuming flow surveys. While computational methods do not yet have the maturity to completely replace the wind tunnel, they nevertheless, when used in parallel with wind tunnel tests, can expand the range of conditions covered and will allow isolation of cause and effect in complicated situations not readily explored even with detailed model build-up testing. The tilt-rotor wake problem is an ideal application for an analysis with off-body calculation capability.

In the past, analytical modeling of the fully coupled rotor/fuselage flowfield models was not possible because of limitations in the computing facilities and the complexity of the separate parts of the calculation. Typically, a rotor wake model or an analytic model of the airframe would each separately fill the available computers. Recently, however, a method has become available which allows the calculation of coupled rotor-airframe behavior. In this approach, developed at Analytical Methods, Inc., under NASA funding, a panel method and a rotor blade element model are run in series, with the connecting links being a panel model of the rotor disc and a time-averaged vortex sheath model of the rotor wake. As the calculation proceeds, the rotor loads are fed (as boundary conditions) to the panel model which solves for the body forces, distorts the rotor wake in the presence of the fuselage and feeds back to the rotor model as updated inflow distributions. The method was first outlined in Ref.1, and has been documented in a number of reports (Refs. 2 through 6). A special feature of the method is that it includes a full calculation of the wake behavior as a routine part of the solution.

The method is incorporated in computer program VSAERO (for Vortex Separation AEROdynamics), which combines the general flowfield modeling capability of panel methods including the determination and representation of regions of separated flow and the interaction of the fixed components of the system with a full blade-element rotor model and rotor wake model, including non-uniform inflow, which is relaxed to reflect the local flowfield. As a consequence, it is possible to determine not only the

effect of rotor downwash on the horizontal and vertical stabilizers, but also the effect of fuselage- and wing-induced upwash on rotor forces and moments. In summary, the program has the capability to determine the fully-coupled aerodynamic response of the airframe/rotor system and, is therefore, an ideal tool to use in the determination of flowfield details.

Before tackling the complex flowfield around the tilt-rotor aircraft, in particular the interaction between the rotor wake and the wing, it was felt that some validation of the analysis on a simpler case was required. Fortunately, an appropriate set of data obtained on a tilt-propeller and wing model tested by NASA (Ref. 7) was available. This report described a series of tests on a semispan wing and tilt propeller at combinations of wing span/chord and chord/propeller radius which were close to the V-22 geometry. In the test, wing angle of attack was varied for selected propeller shaft tilt angles over a range of thrust and propeller advance ratios. Force and moment data were taken for each condition.

Four of the cases selected for analysis by VSAERO are presented in this paper. All are with the nacelles at 90° and the wing at 0° angle of attack and cover a range of flight conditions in the helicopter mode (edgewise flight) from hover to an advance ratio of 0.14.

The second part of the study involves the analysis of a representative tilt-rotor configuration. Based on early V-22 wind tunnel model lines, a numerical model was constructed to represent the aircraft in both helicopter and fixed wing modes and was run for a range of conditions from hover through transition as a helicopter and up to 140 knots as an aircraft. Only the helicopter results are reviewed here. The details of the wing/rotor wake interactions are described including distributed airloads and integrated forces and moments.

Technical Approach

The VSAERO program uses a low-order panel model to describe the surface of the configuration under study. Each panel is represented by a compound singularity made up of a doublet and a source term. The source term is used simply to "unload" the singularity, as it is set to the normal component of

the free stream velocity and is known. The doublet term, the unknown, is therefore, of lower strength leading to a better conditioned solution. A Dirichlet, internal potential, boundary condition is applied. The output of the solution is the doublet strength, a scalar. The velocity field is determined by carrying out a surface differentiation of the doublet distribution after the solution is complete. Wakes are modelled by doublet sheets attached along the appropriate shedding line and may be relaxed to the correct, force-free location in the stream as an integral part of the solution.

Two approaches to modelling rotors and propellers are available. In the first, described in detail in Ref. 5, the rotor wake is represented by a time-averaged vortex sheath fed by a panel model of the rotor disc. The boundary conditions on the disc are completely described by the output of a blade element model of the rotor which feeds time-averaged loading as a function of radius and azimuth to the panel model. Beginning with an assumed uniform inflow, the program iterates between the blade element model and the panel model, feeding loading one way and inflow velocity the other way. Convergence is established when wake shape, strength, and inflow stabilize.

For an application where detailed blade loads are required this approach would be used. In the present case where the effect of the rotor on the body is of primary interest, a simpler approach is available. Here, the rotor wake is still modelled with a vortex sheath but the loading is prescribed. Using a simple segmented actuator disc approach and momentum theory, the rotor flow-through is determined. This may be modified, as in the present case, to represent radial and azimuthal variations by using a simple Glauert distribution (Ref. 8). With rotor inflow set as a function of thrust and flight speed, the initial wake shape is assumed to be a simple skewed sheath with the wake strength determined by the requirements of the momentum theory. The calculation then proceeds to determine the effect of the rotor on the fuselage and wings and the coupled influence on the rotor wake. This approach has been shown to produce representative results for both rotor and propeller flow fields and is the preferred approach, for reasons of economy, when detailed blade loads are not required.

Preliminary Correlation Study

The dimensions of the NASA wind tunnel model of the propeller/wing are presented in Fig. 1 taken from Ref. 7. The panel model of this configuration is shown in Fig. 2 The wing was modelled with 8 panels chordwise on the wing upper and lower sufaces and 8 panel rows spanwise. The wing tip was closed. The nacelle is a simple body of revolution with 12 panel intervals around the circumference. The propeller model follows the nacelle panelling with 12 azimuthal divisions and has 5 radial panels spaced more closely towards the rotor tip.

The initially prescribed wake for the forward flight cases was attached around the rotor disc edge and the wing trailing edge as shown in Fig. 3. Since the nacelle aft side will be separated, this zone was also modelled, enclosed with a wake, as is also shown in Fig. 3. The extent of the separated flow region could have been readjusted as the flow calculation proceeded. However, this would have required that a streamline and boundary layer calculation be made at each step, and that the line of separation be reset to the new value each time. This extra complexity was felt to be unjustified for the purposes of the study.

In program VSAERO, conditions are set by specifying the normal velocity on a panel as a function of some reference velocity, normally free stream, or, in the case of a hover condition, the average momentum inflow velocity. From Ref. 7, all the correlation cases were run at a nominal slipstream dynamic pressure (q_s) of 8 pounds per square foot. Following the definition of propeller thrust coefficient,

$$C_{Ts} = \frac{T/A}{q_s} .$$

where

$$q_s = q_\infty + T/A = 8$$

and hence, $$q_s(1-C_{TS}) = q_\infty$$

Also, in helicopter notation,

$$C_T = T/\rho A V_T^2$$

$$\mu = V_\infty/V_T$$

and therefore $$C_T = \frac{C_{Ts}\mu^2}{2(1-C_{Ts})}$$

From these simple expressions and assuming sea level standard conditions, the values in Table 1 may be developed. The values of w and v come from simple momentum theory illustrated in the sketch accompanying Table 1. Wake inner velocity , Vs, is the vector sum of V_∞ and w; V_0 (wake outer velocity) is the "wakewise" component of V_∞.

The values of v, V_s, and V_0 are used as input to program VSAERO and determine the wake strength. The initial position of the wake from the propeller is set using the momentum valve of wake deflection, θ, as a guide. In each case the calculation proceeded from the initially prescribed settings to a stable wake. Two iterations were found to be adequate.

Program VSAERO was run for each of the four conditions outlined in the table and the details of the results are presented in Figs. 4 through 7. In Fig. 4 the calculated forces and moments are superimposed on the measured data taken from Ref. 7. For the edgewise flight conditions examined ($i_p = 90°$), correlation is generally excellent for both forces and moments, with the sole exception being the highest advance ratio case ($\mu = 0.14$, $C_{Ts} = 0.6$). Even here the calculated results follow the general trend of the experiment. Only one data point caused concern and is not plotted in Figure 4. That is the calculated pitching moment at $C_{Ts} = 0.9$. Here, although the calculated force values agree well with experiment, the calculated moment was "off-scale." The cause was not determined but appears to be related to the initially assumed wake shape. If the assumed wake was typical of a higher speed, forward flight case one value was found; if a low speed wake was assumed, another moment value was calculated.

Since the lift and drag values did not change significantly, some distributional effect related to the wing/propeller interference must be inferred. The condition appeared to be unique to the $C_{T_S} = 0.9$ condition since it was not present for the other three cases.

Figs. 5 are a selection of wake visualization studies of the three forward flight cases. Pictured on the drawings, in addition to the panel model of the wing, nacelle, and propeller are the streamwise elements of the doublet panels used to construct the wake. An initially prescribed wake (already illustrated in Fig. 3) is allowed to deform under the influence of the propeller and the fixed components. The wake strength is determined by the local disc loading (the lateral elements) and the azimuthal variation in loading (the streamwise elements). The rather coarse wake development is a result of using a large spacing between the wake calculation grid planes in the interest of computational economy.

Because of the complicated interaction between wing and propeller wake, it is difficult to establish what goes where from the overall views. To clarify the situation, Fig. 6 presents cross sections through the wakes showing only the wing and propeller components. Except for the hover condition ($C_{T_S} = 1.0$), where the wing is fully involved in the propeller wake, all three forward flight wakes exhibit a common characteristic. That is, the inner portions of the wake are lifted up above the wing root plane while the outer portions curl under and are convected downward by the general propeller flow. Fig. 6(b), for $C_{T_S} = 0.9$, is the best example of this behavior.

The reason for this somewhat unexpected trend is found in the span loading distributions of the wing at the three forward flight advance ratios shown in Fig. 7. In each case the wing outboard is downloaded, while the inboard portions of the wing are lifting. Knowledge of the loading allows construction of a schematic model of the vortex field behind the wing such as Fig. 8, showing the vortices at a given streamwise location at the disc trailing edge. It can be seen that, depending on the balance of strength between the rotor inboard vortex, R_I (the rotor is being assumed to act like a low aspect ratio wing) and the wing mid-span vortex, W_M, flow in the root region can be either up, R_I stronger than W_M , or down, R_I weaker than W_M.

Also, the vortex pair will rotate and/or track differently depending on their relative location and strength. From flight tests of the XV-15, the downloading effect of the rotor wake on the wing vanishes at about 40 knots (μ =.054) and C_{T_S} =.88. This agrees with the results of Fig. 7 which shows the net wing force to change from a download to a lift at an advance ratio slightly greater than .043 at C_{T_S} < .90.

In reviewing the filament diagrams of the wakes (Fig. 5) it should be remembered that they represent the outer envelope of the rotor induced flow field and should not be confused with the more familiar (in rotary wing aerodynamics) time-varying pictures of rotor tip vortex wake filaments. However, when taken together, the streamwise and crosswise edges of the elements making up the wake sheath do, in fact, represent the time-average effects of the tip filaments.

V-22 Tilt-Rotor Configuration Study

Fig. 9 shows the panel model of an early V-22 tilt-rotor wind tunnel model used for the correlation study. All of the fuselage and wing detail, with the exception of the tail assembly, is represented including the wing and rotor wakes and the separated flow wake behind the nacelle and the nacelle base wake. As with the work on the propeller-wing model discussed above, a simple momentum model of the rotor wake was used and only rotor on fuselage and wing effects were determined. Table 2 outlines the flight conditions for which calculations were made. Note that the flaps are not deflected in the panel model whereas, on the aircraft, flaps are extended in the low-speed conversion mode. This was done for ease of modelling. Note also that the thrust coefficient used in Table 2 now follows the rotor convention, $C_T = T/\rho A V_T^2$.

In hover, the fuselage and nacelle presence contributes little to the overall wake dynamics, with the flow being controlled by the wing/rotor interaction. This has been explored in considerable detail in Ref. 9 and will not be covered here. Instead, attention will be focused on the transition cases since they represent the progressive breakout of the wing

from the influence of the rotor wake as the aircraft enters forward flight. In Fig. 10, cross sections of the rotor wake are plotted as they pass through the plane of the wing mid-chord. Wakes for 15, 30, 45, and 60 knot cases are superimposed. At 15 knots the outboard portion of the wing is fully immersed in the rotor wake. At 30 knots and 45 knots the wing is still in contact with the wake and it is not until about 60 knots that the rotor wake lifts completely clear of the wing. Even here, however, with no direct wake interference present, the outer portions of the lifting surface still experience a download due to the slipstream deflection.

Fig. 11 shows the progressive development of the wing/rotor wake. Note particularly the development of the wing wake, curling up and over on the inboard end and down and under on the outboard end, reflecting the rotor induced changes in loading. Because of the influence of the rotor, the wing for all these conditions is carrying a download on its outboard end. Note also the strongly asymmetric shape of the wake cross section and the upward convection of both wing and rotor wake against the plane of symmetry.

The wing/rotor flowfield for these low advance ratios is very complicated. This is well illustrated in Figs. 12(a) through (d). Here, general views of the full configuration at 45 knots are presented followed by views where the wing and rotor wakes are drawn separately. These highlight the way in which the wing and rotor wakes interact, with the inboard portions of the wake being picked up and rolled into the inboard rotor edge bundle. As might be expected, with the negative loading on the outer portion of the wing, the wake rolls under rather than over. Notable also is the tendency for the inboard rotor wake to be carried upward under the influence of its reflection in the plane of symmetry in the analytical model, and by its port side counterpart in the real world as it moves aft.

The total forces and moments on the model were determined by integrating the theoretical distributed airloads including all the wake interference terms. Fig. 13 shows the variation of estimated airframe (tail off) download-to-thrust ratio with airspeed during conversion. Note that this is not truly representative of the aircraft since conversion is normally accomplished with flaps set to 40°, not to 0°.

In hover, the computed download/thrust is 13 percent, flaps up. This value decreases during transition until the download is zero at about 80 knots. The calculations show an increase in download at 45 knots. This value is unexpected in view of the smooth way in which the fuselage attitude, wing-in-slipstream angle-of-attack, and thrust vary. The precise reason for the behavior at 45 knots is being examined. The computed drag, shown in Fig. 13, includes only pressure drag and induced drag terms. No skin friction contribution has been included. The rotor contributions have been removed, so the terms represent the airframe loads only.

As with the download, at low speed the drag is dominated by the wing. This results from the high leading-edge suction developed on those parts of the wing in the rotor wake. The suction falls off almost linearly until the wing breaks free of the slipstream at about 35 knots. Once exposed to the free stream, a drag is generated. The existence at this forward thrust in hover has the interesting implication that, were the aircraft to hover with flaps up, a small rearward tilt of the rotor discs would be required to remain stationary.

Conclusions

The primary objective of this study was to investigate the behavior of the dynamics of the wakes from the wing and rotor of a typical tilt-rotor aircraft in transition flight.

The results of the analysis of a simple wing/tilt-propeller configuration showed excellent correlation with measured values of total forces and moment throughout the speed range. This provides indirect validation of the program's ability to explore the wake dynamics since if the wake model were not correct, correlation of the forces and moments would be unlikely.

When applied to a representative tilt-rotor configuration, the analysis showed the complex interaction between the rotor and wing wakes and illustrated clearly the flowfield at the tail. The wake behavior follows expected trends and echoes results found in the propeller-wing study. The results show that the VSAERO program has demonstrated its ability to model

the complex flow interactions involved in the tilt-rotor aircraft and is therefore an ideal tool for application in the configuration development phases of the design process.

Acknowledgements

The authors would like to acknowledge the contributions of their colleagues at AMI and at Bell-Boeing. Financial support for the analytical portions of this work was provided by Bell-Boeing under Purchase order M/SP30-74.

References

1. Clark, D.R., An Outline of a Method for Predicting Fully Coupled Body/Rotor Interference, Paper Presented at ARO Workshop on Rotor Wake Technology, Raleigh, N.C., 1979

2. Clark, D.R. and Maskew, B., An Analysis of Airframe/Rotor Interference in Forward Flight, Paper Presented at 7th European Rotorcraft and Powered Lift Forum, Garmisch-Partenkirchen, FRG, September 1981.

3. Clark, D.R. and Maskew, B., Calculation of Rotor/Airframe Interference for Realistic Configurations, Paper No. 2.6, Presented at 8th European Rotorcraft and Powered Lift Aircraft Forum, Aix-en-Provence, France, September 1982.

4. Clark, D.R. and Maskew, B., Aerodynamic Modeling of Helicopter and Tilt-Rotor Configurations, Paper Presented at 39th Annual Forum of the AHS, May 1983.

5. Clark, D.R., Study for Prediction of Rotor/Wake/Fuselage Interference: Parts I and II, NASA CR-16653-I, NASA CR-16653-II, November 1983.

6. Maskew, B., Prediction of Subsonic Aerodynamic Characteristics: A Case for Low-Order Panel Methods, J. Aircraft, Vol. 19, No. 2, February 1982.

7. Spreeman, K.P., Investigation of a Semispan Tilting Propeller Configuration and Effect of Ratio of Wing Chord to Propeller Diameter on Several Small-Chord Tilting Wing Configurations at Transition Speeds, NASA TN D-1815, July 1968.

8. Johnson, W., Helicopter Theory, Published by Princeton University Press, 1980.

9. Clark, D.R., Analysis of the Wing/Rotor and Rotor/Rotor Interactions Present in Tilt-Rotor Aircraft, Paper Presented at the International Conference on Rotorcraft Basic Research, ARO, Durham, N.C., February 1985.

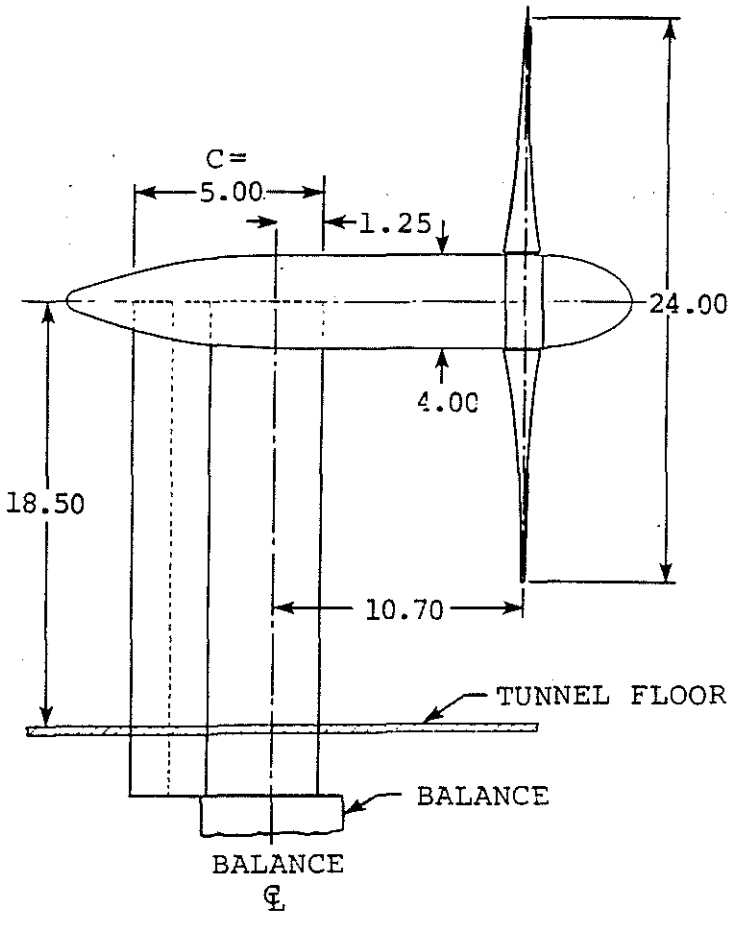

Figure 1. Diagram of Prop/Wing from Spreeman (Ref.7)
(Dimensions in inches)

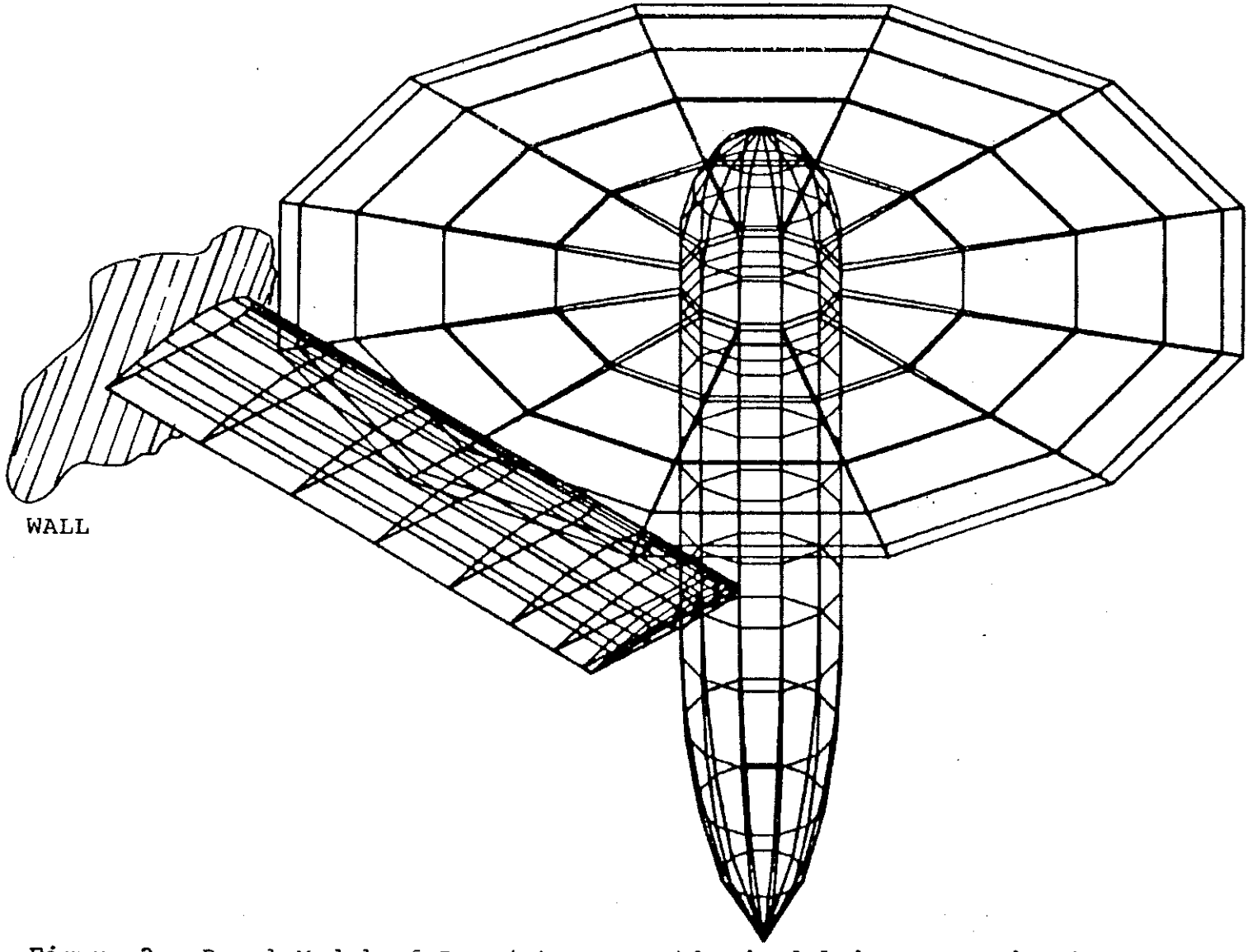

Figure 2. Panel Model of Prop/Wing Assembly (Model is symmetric about wall plane)

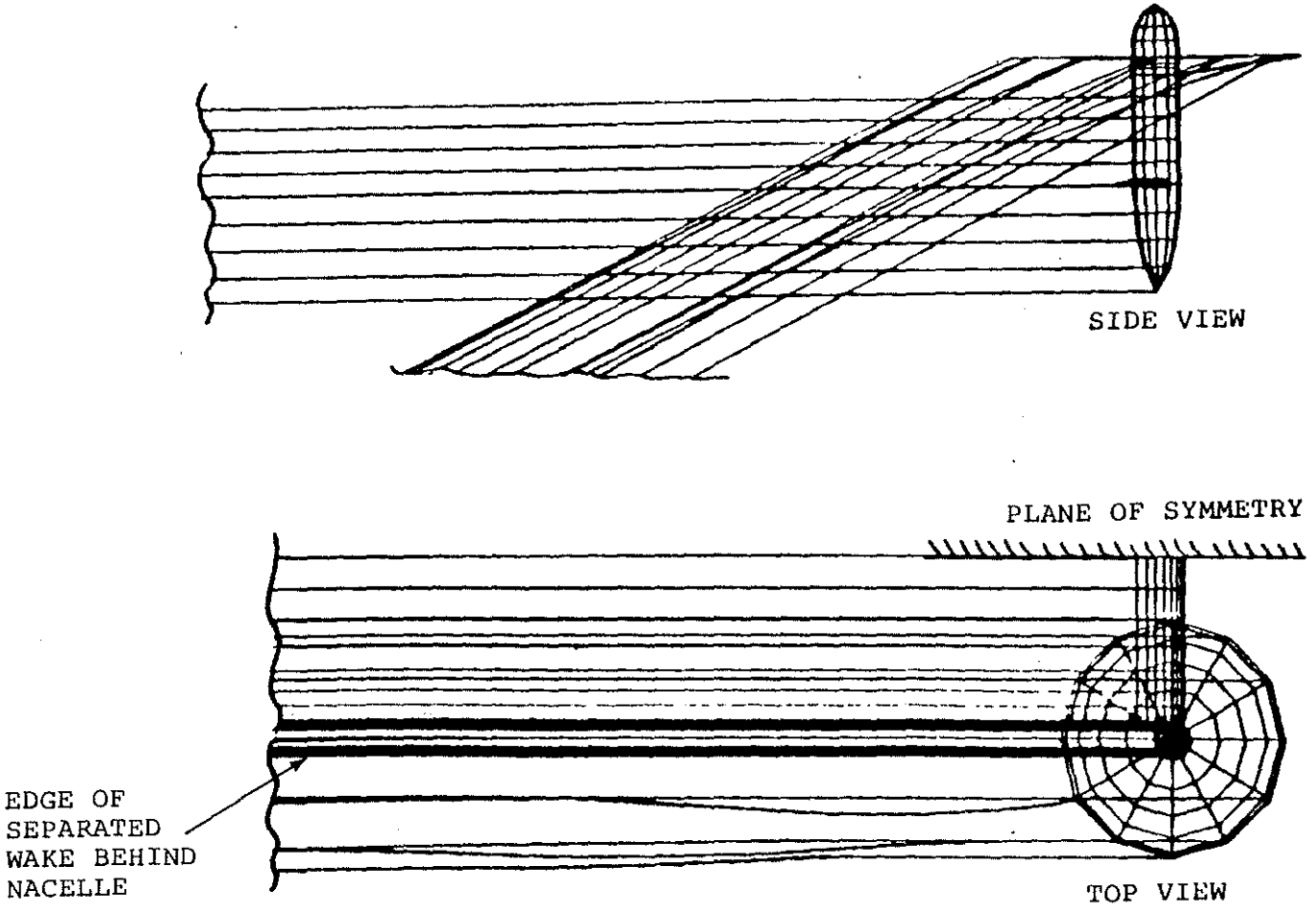

Figure 3. Typical Prescribed Wakes [Calculation Starting Condition].

Table 1. Summary of Calculated Conditions

C_{T_S}	T/A	C_T	V_S	V_o	V_∞	$w = 2v$	θ	μ
1.00	8.0	0.0130	82.0	0.0	0.0	82.0	0.0	0.0
0.98	7.8	0.0129	79.6	1.66	11.5	78.8	8.3	0.023
0.90	7.2	0.0083	83.3	8.05	25.9	79.25	18.1	0.043
0.60	4.8	0.0147	81.0	33.09	51.8	62.31	39.7	0.14

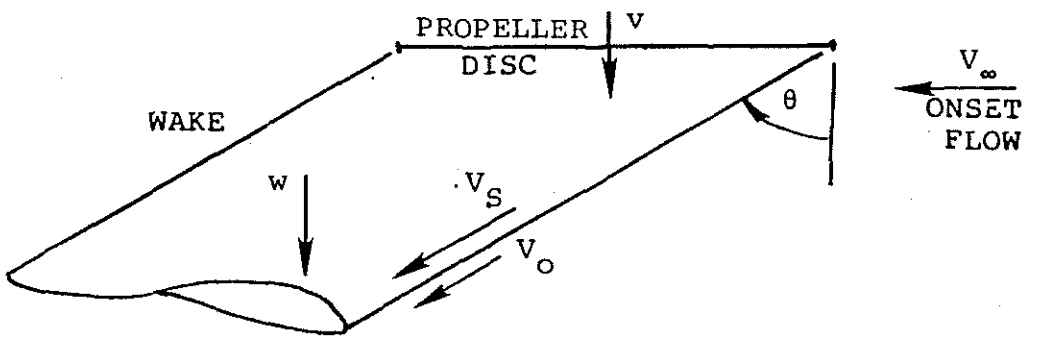

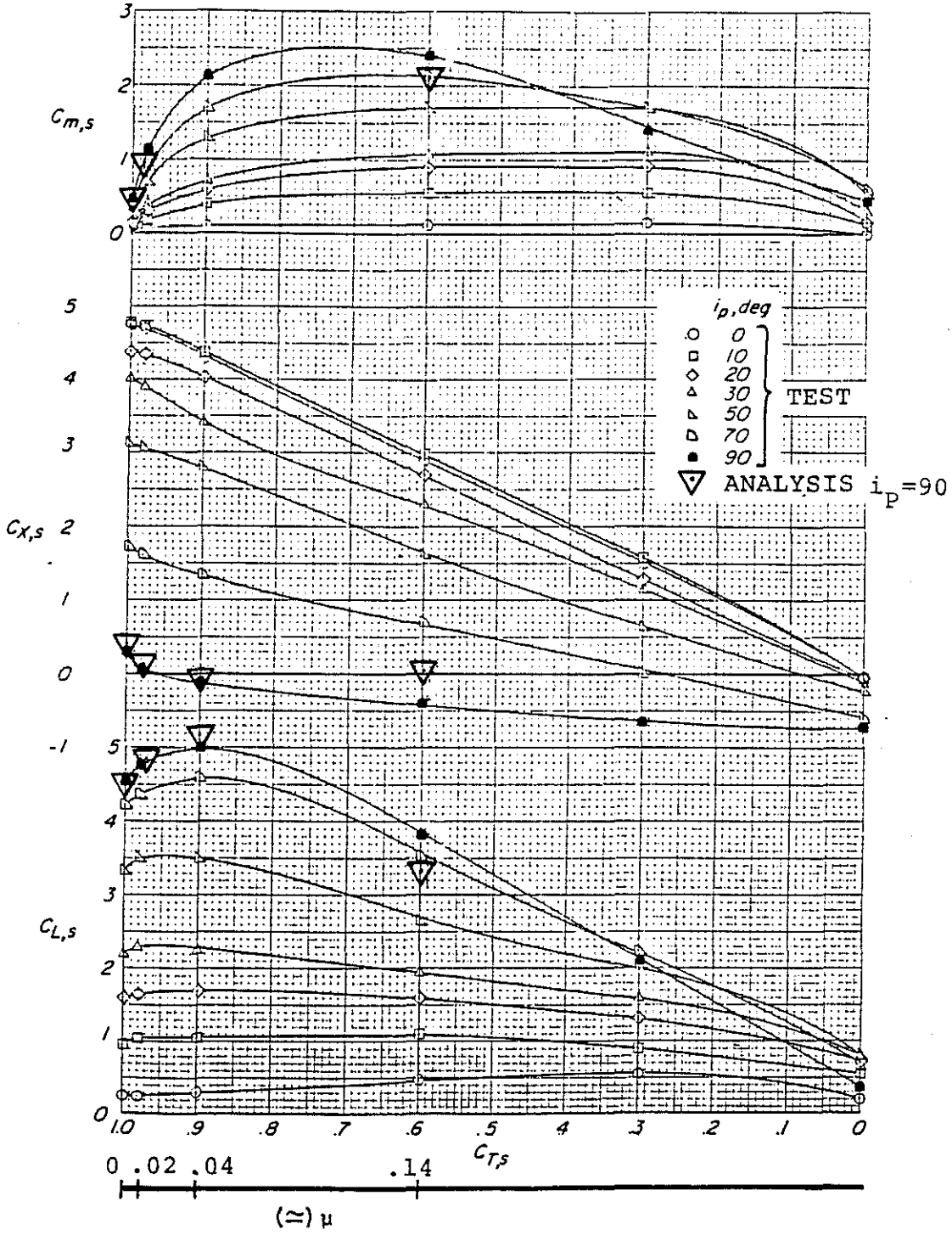

Figure 4. Correlation of Measured and Calculated Integrated Forces and Moments (Using Figure 9(a) from NASA TND1815); $\alpha_W = 0°$

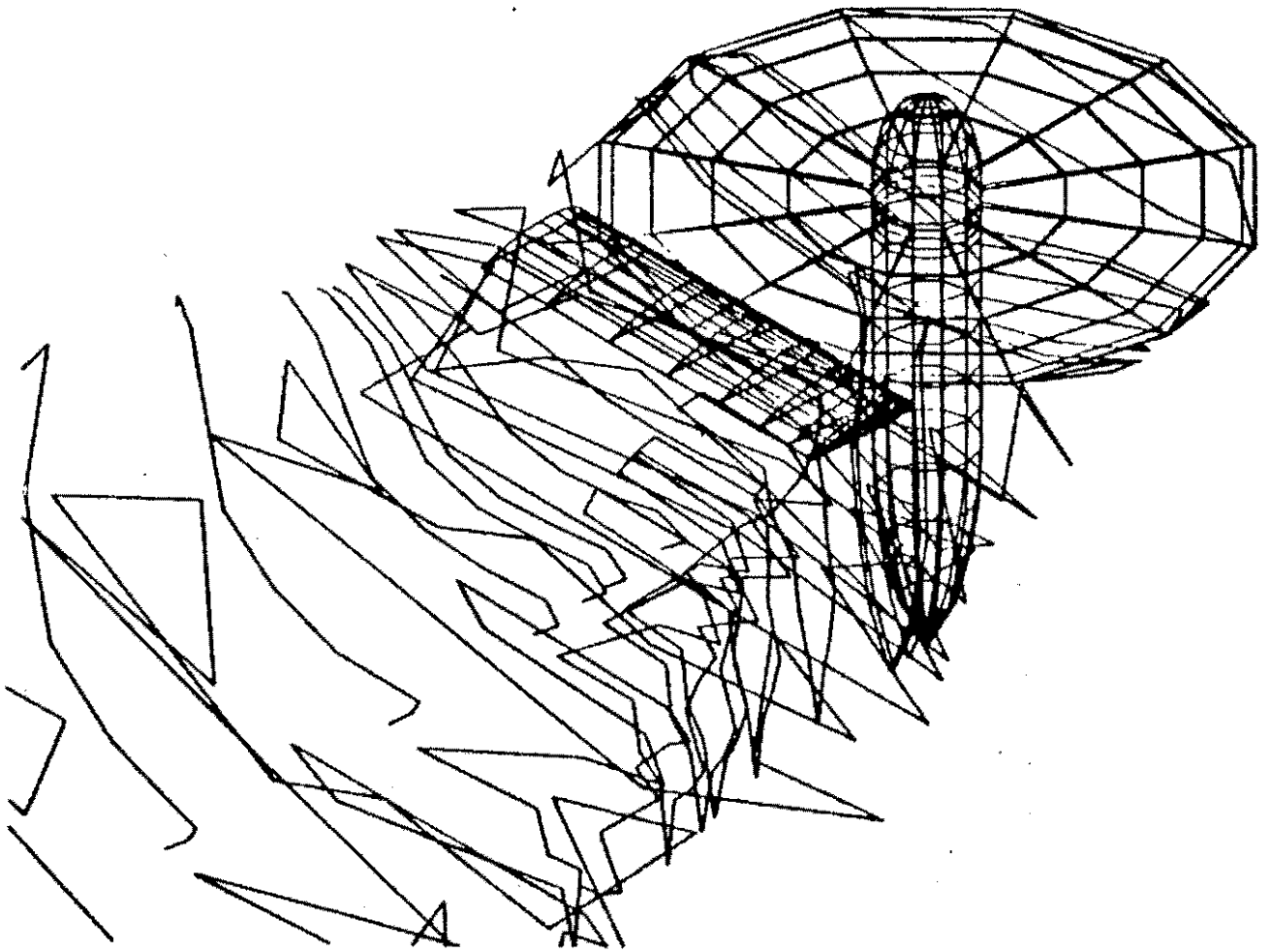

Figure 5(a). Typical Wake Picture - $C_{T_S} = 0.9$, $\mu = 0.043$
(Only Transverse Wake Elements Shown)

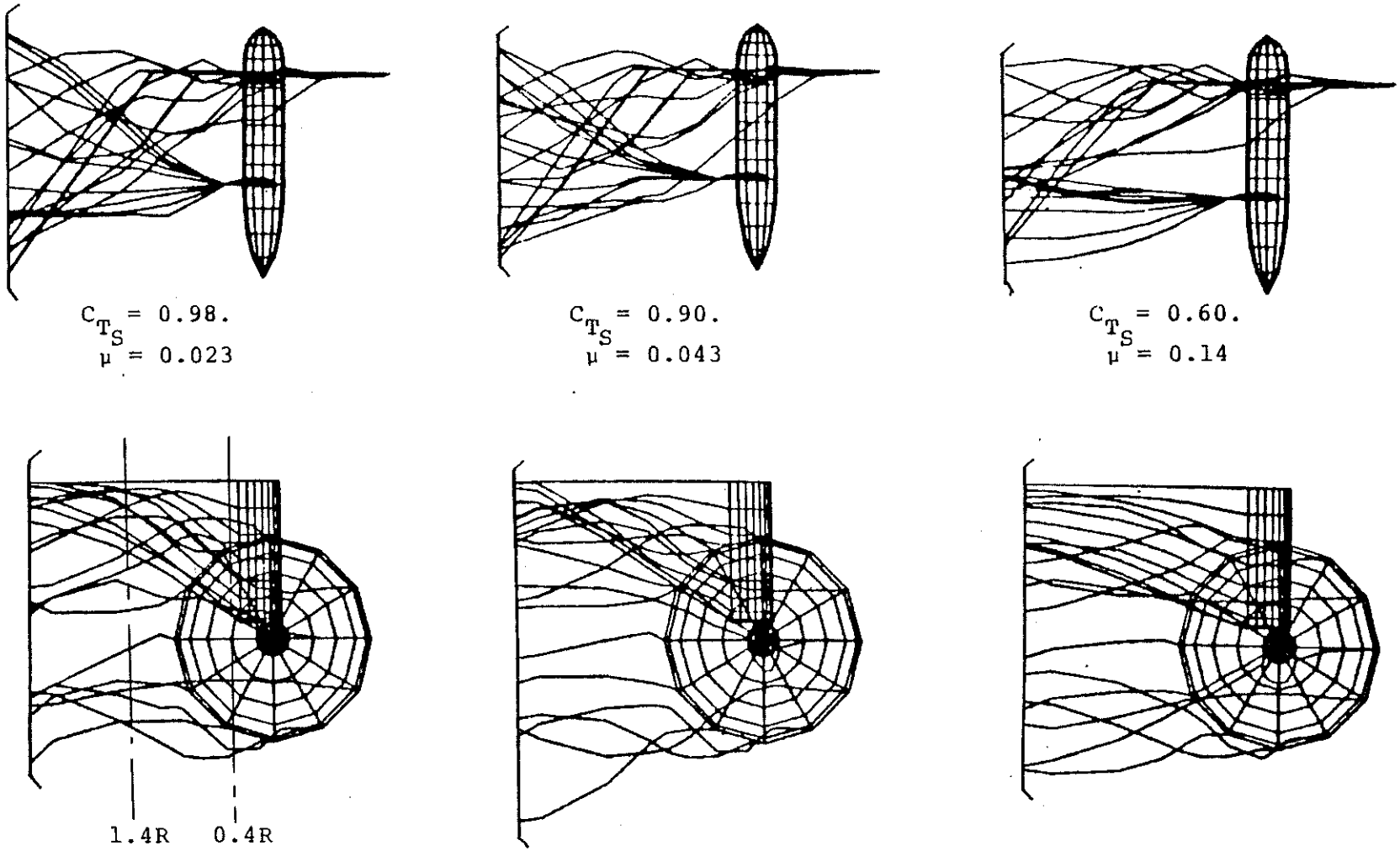

Figure 5(b). Calculated Wake Shapes for the Wing/Propeller Model of Ref. (7)

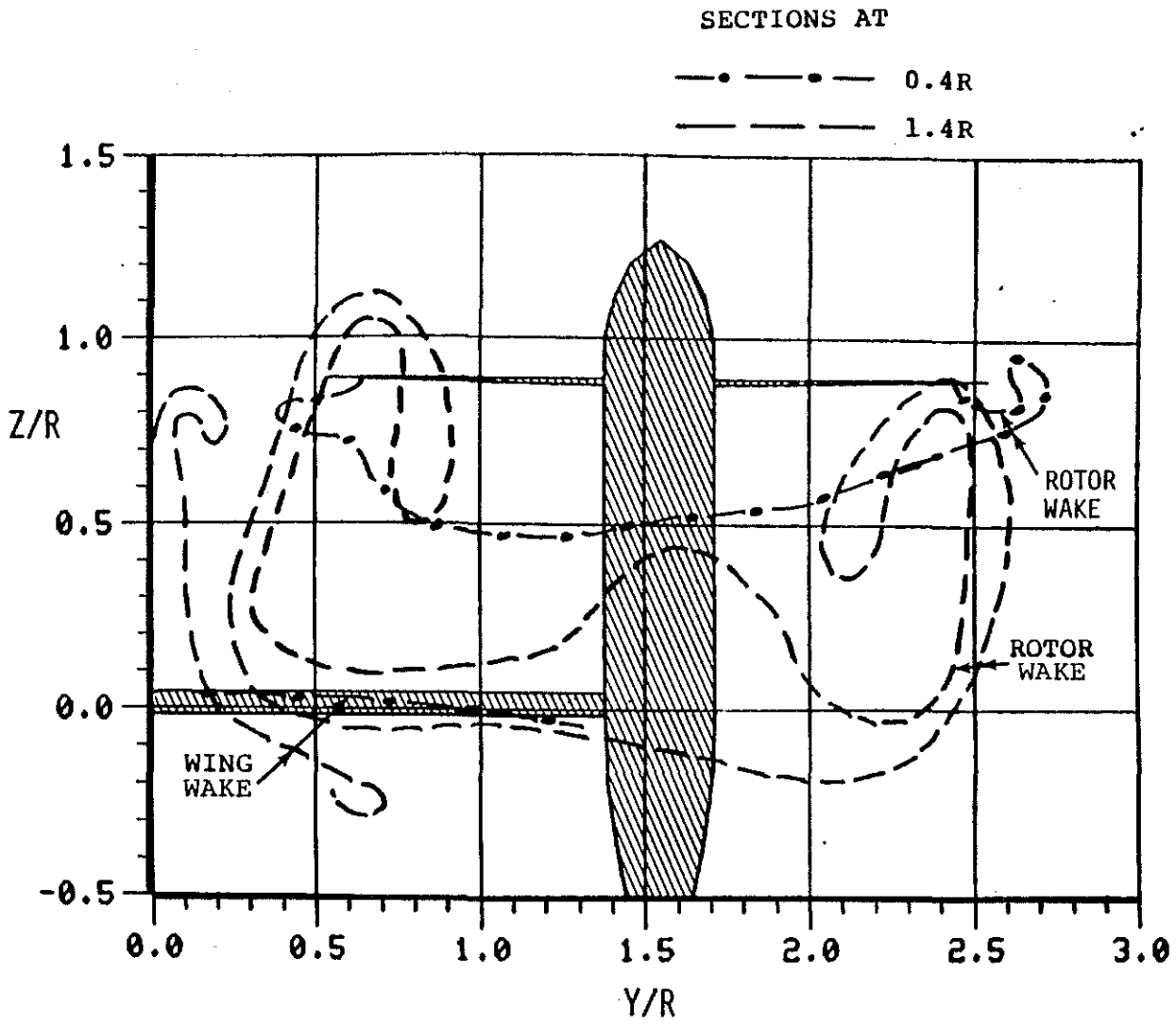

Figure 6(a). C_{T_S} = 0.98, μ = 0.023, Wing and Rotor Wake Cross Sections

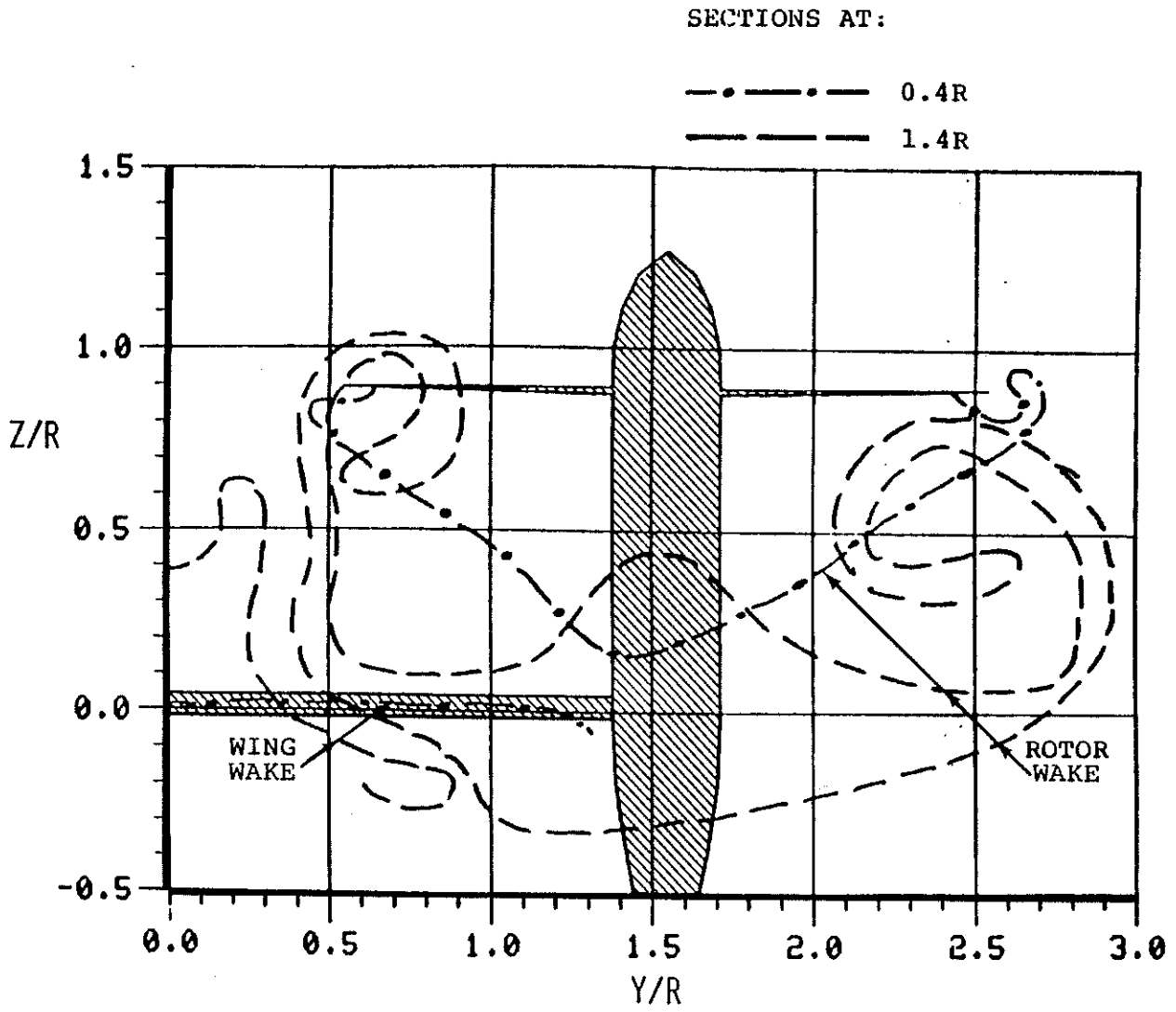

Figure 6(b). C_{T_S} = 0.90, μ = 0.043, Wing and Rotor Wake Cross Sections

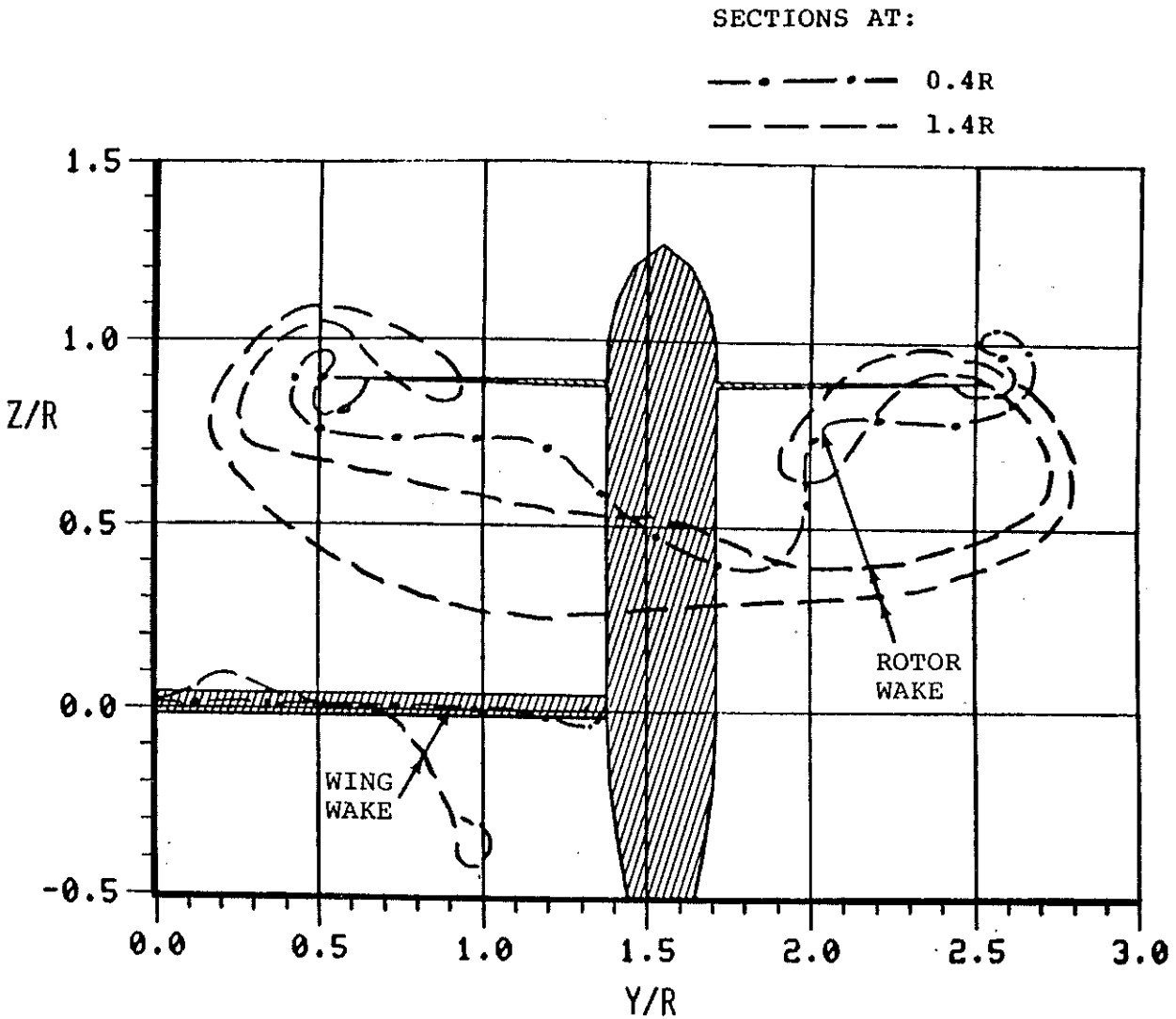

Figure 6(c). C_{T_S} = 0.6, μ = 0.14, Wing and Rotor Wake Cross Sections

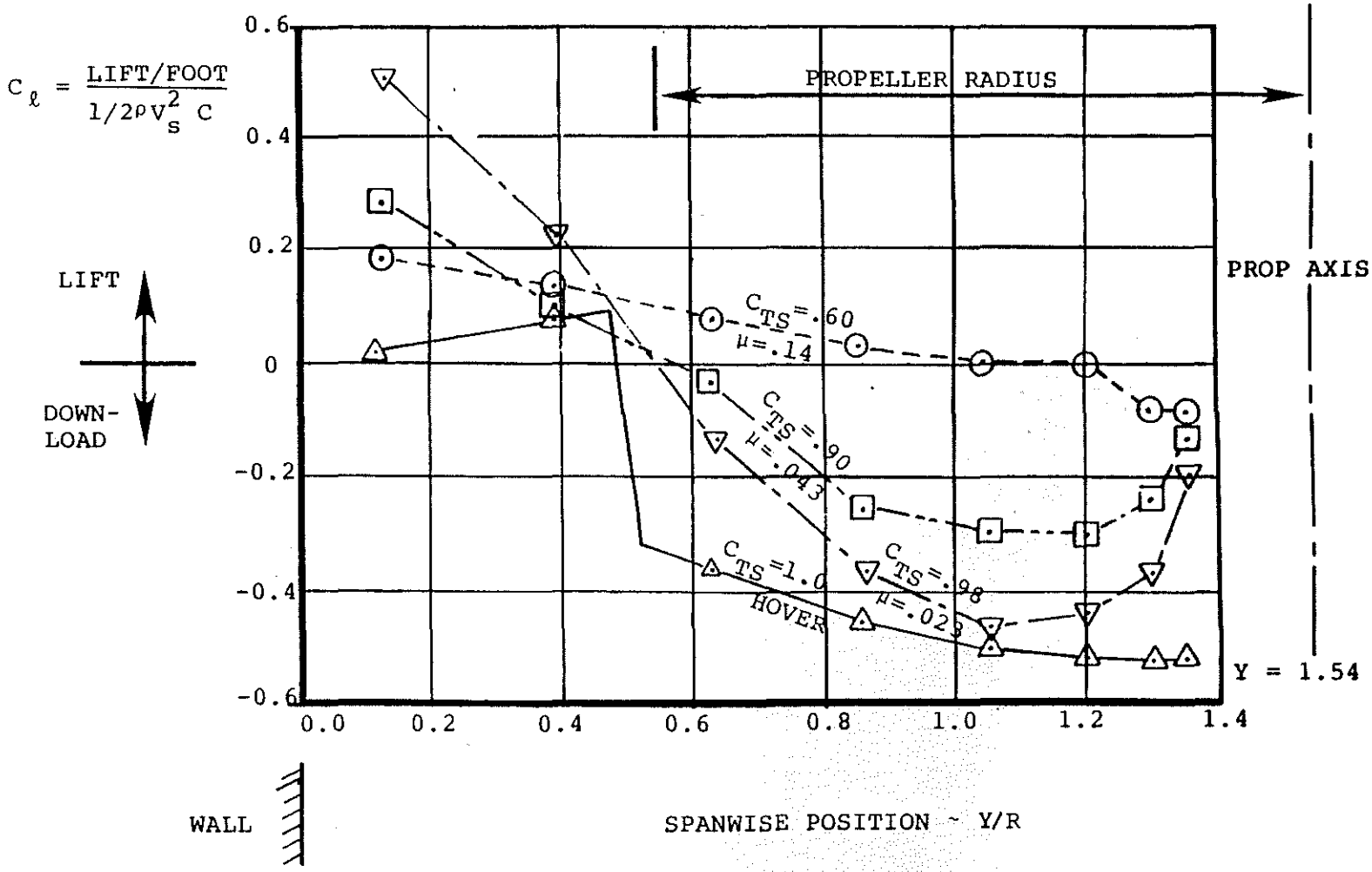

Figure 7. Calculated Variation of Wing Loading with C_T.

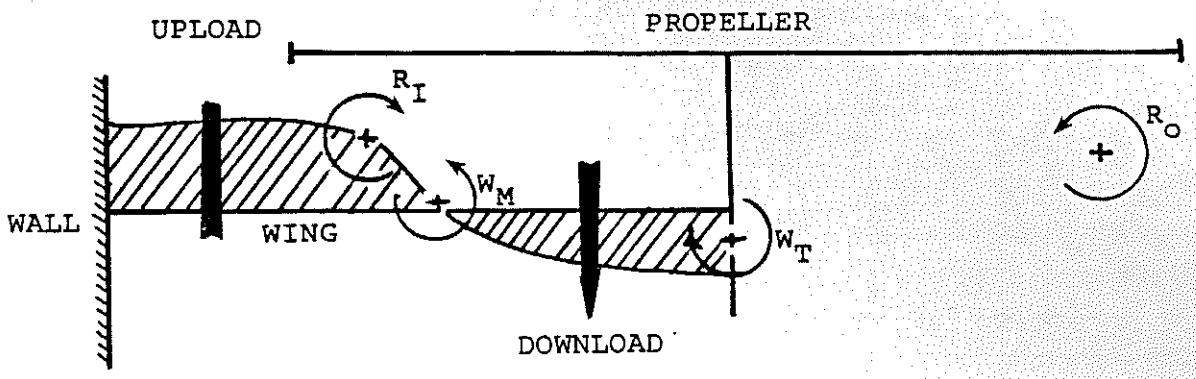

Figure 8. Schematic of Wing-Propeller Vortex Wake

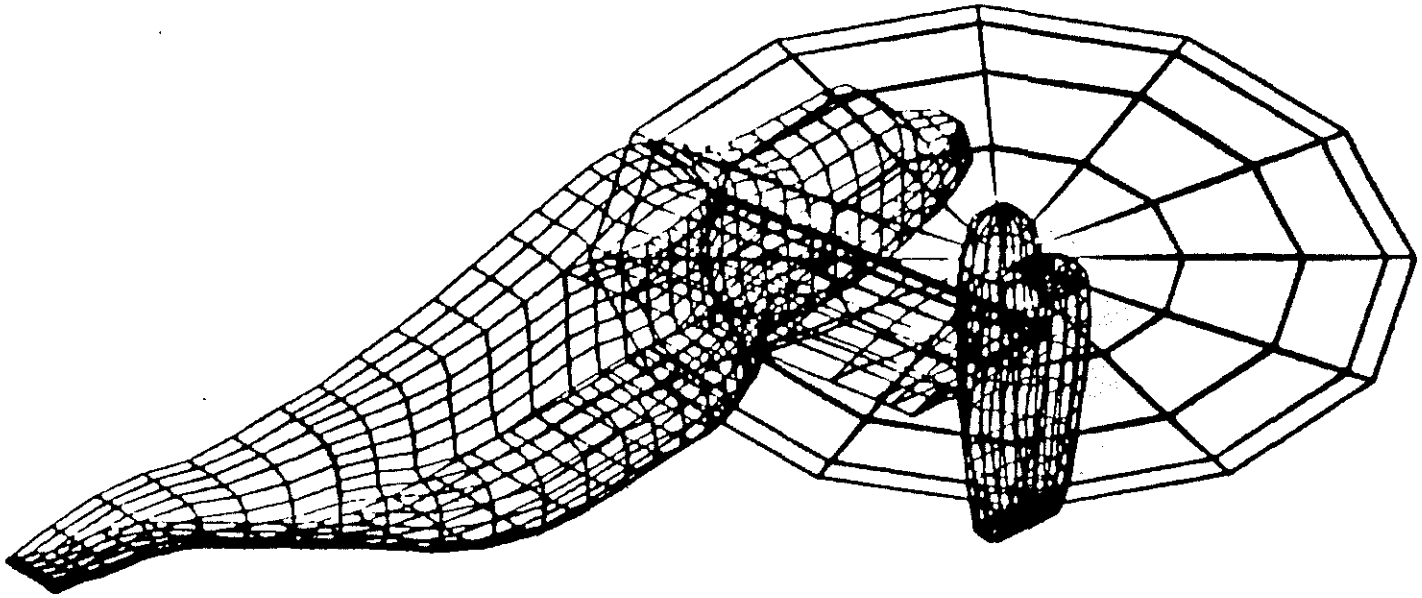

Figure 9. Panel Model with Rotor Disc Added

Table 2. List of Flight and Rotor Parameters at Each Condition Calculated

CONDITION	MODE	AIRSPEED (Kts)	ANGLE OF ATTACK (Deg)	NACELLE ANGLE (Deg)	C_T
1	Rotor	15	2.0	90	0.016
2	Rotor	30	0.5	90	0.0120
3	Rotor	45	-1.5	90	0.0115
4	Rotor	60	-3.0	90	0.0110

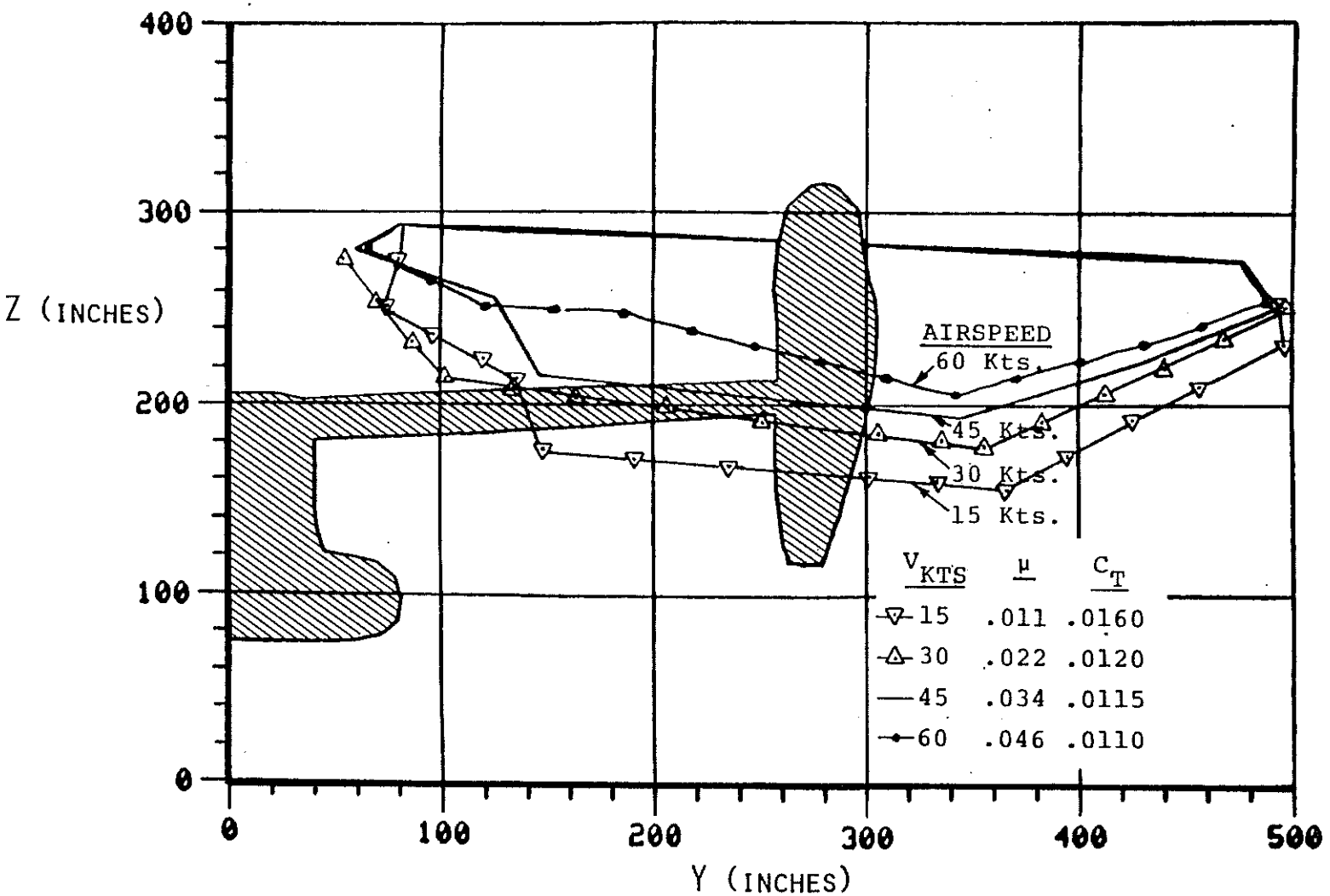

Figure 10. Wake Cross Sections Near Wing Mid-Chord

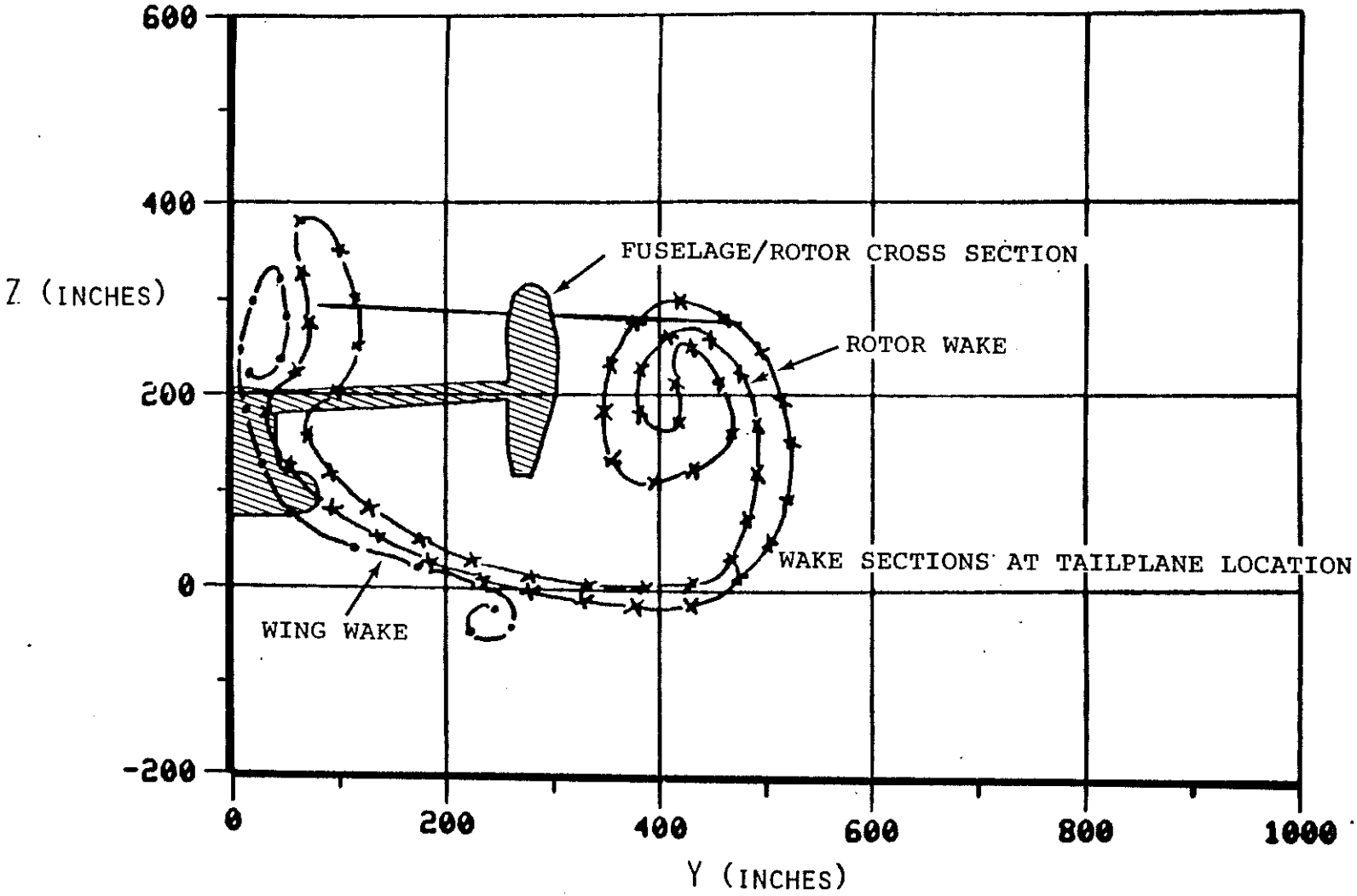

Figure 11(a). Rotor and Wing Cross Sections at Tail Location
(Airspeed 30 Kts, $\alpha = -0.5^{\circ}$, $C_T = 0.012$)

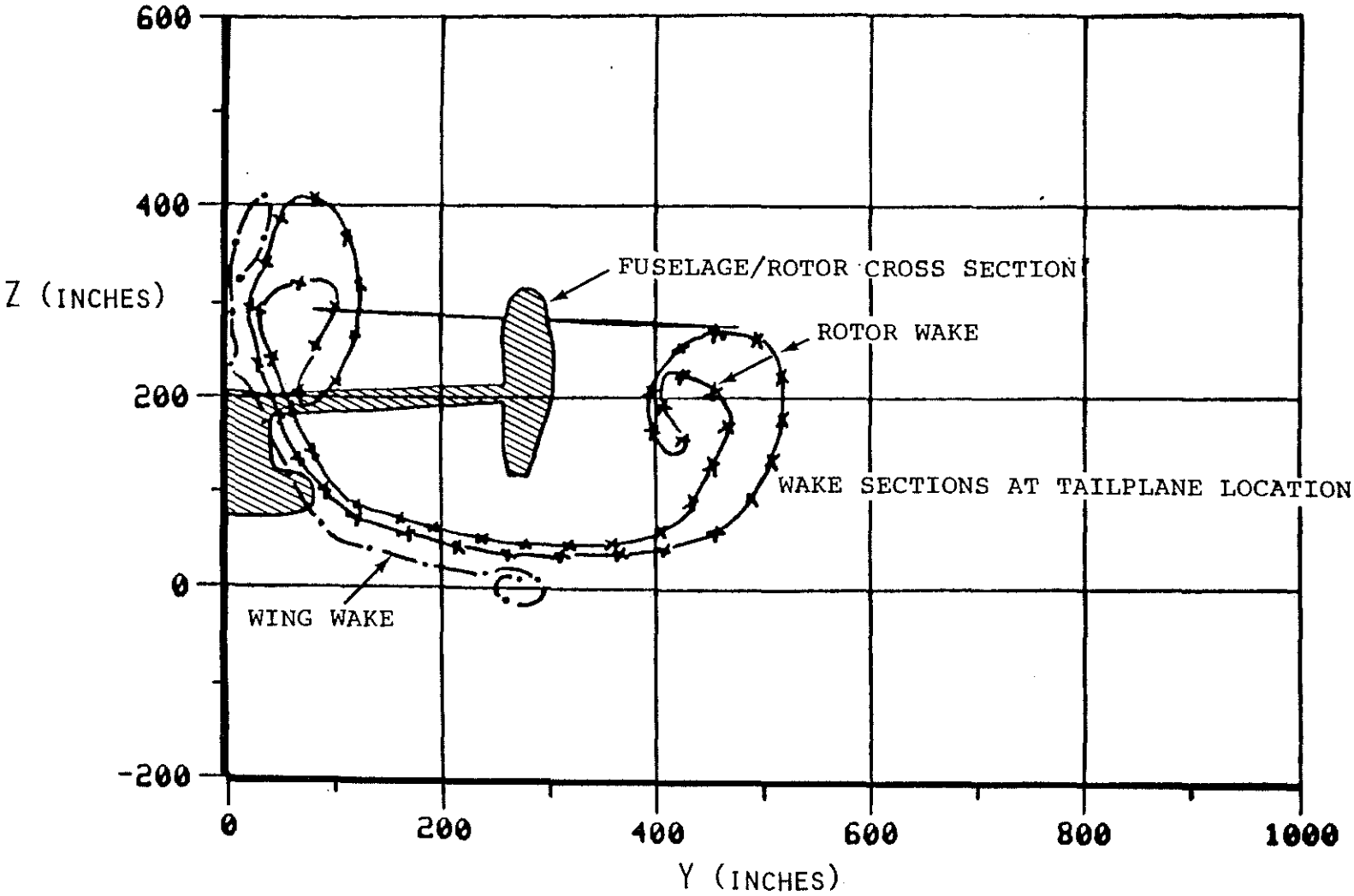

Figure 11(b). Rotor and Wing Cross Sections at Tail Location (Airspeed 45 Kts , α= -1.5°, C_T= 0.0115)

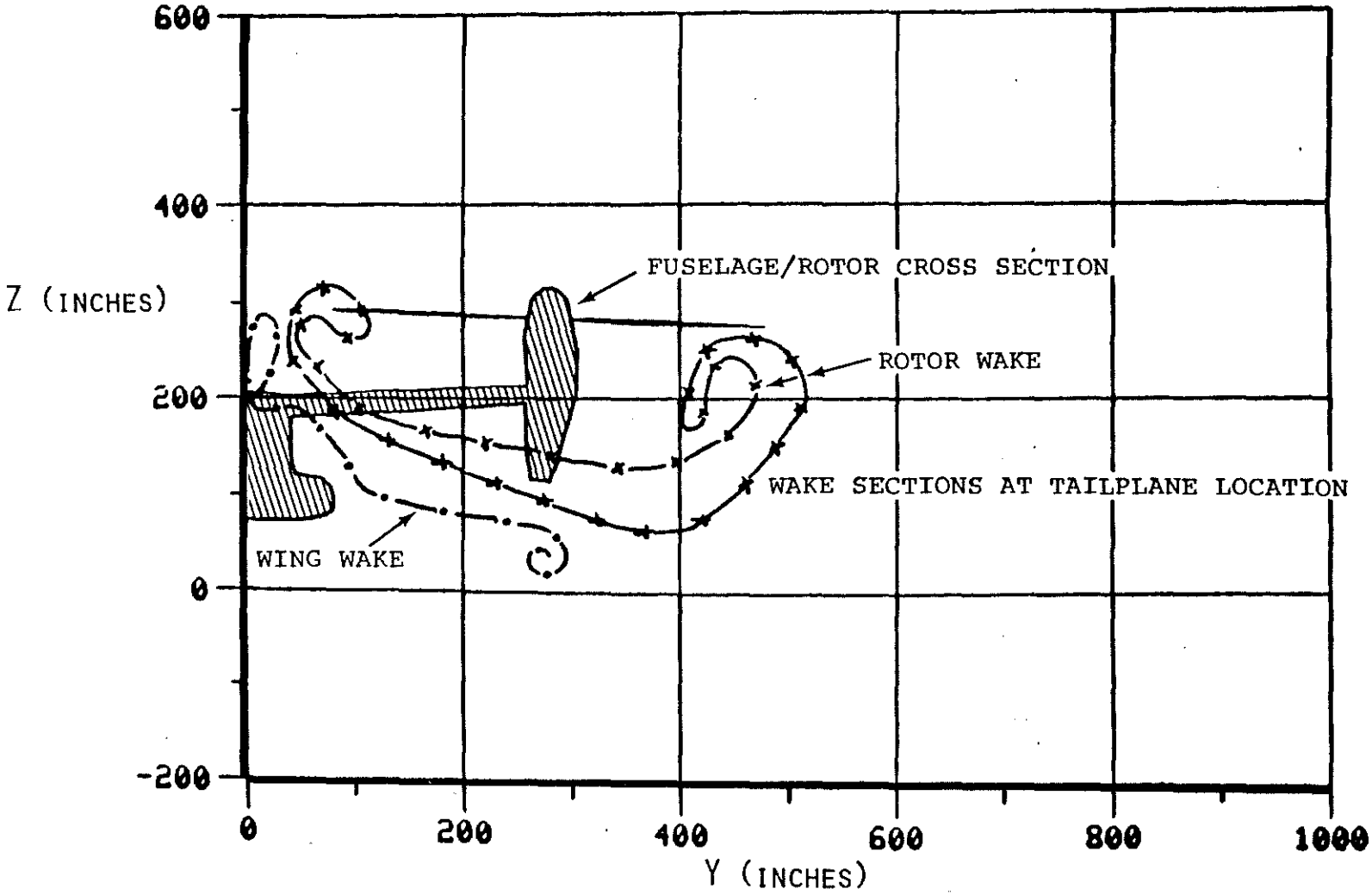

Figure 11(c). Rotor and Wing Cross Sections at Tail Location
(Airspeed 60 Kts, $\alpha = -3.0^{\circ}$, $C_T = 0.011$)

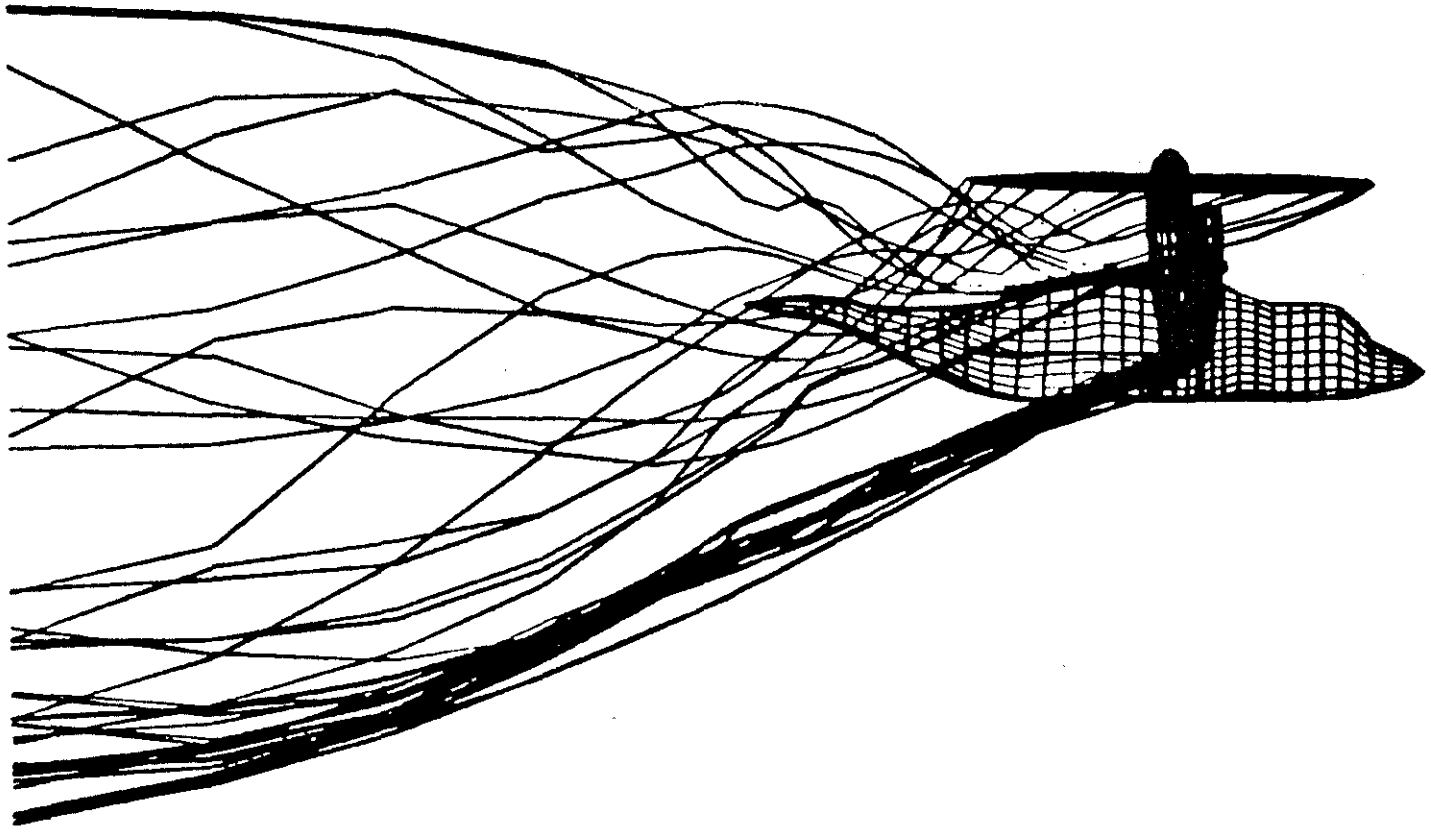

Figure 12(a). Details of the Overall Wake Structure for a Typical Transition Flight Condition; Airspeed 45 Kts, $\alpha = -1.5°$, $C_T = 0.015$

General View of Full Wake Including Engine Exhaust. Wakes Drawn with Streamwise Filaments.

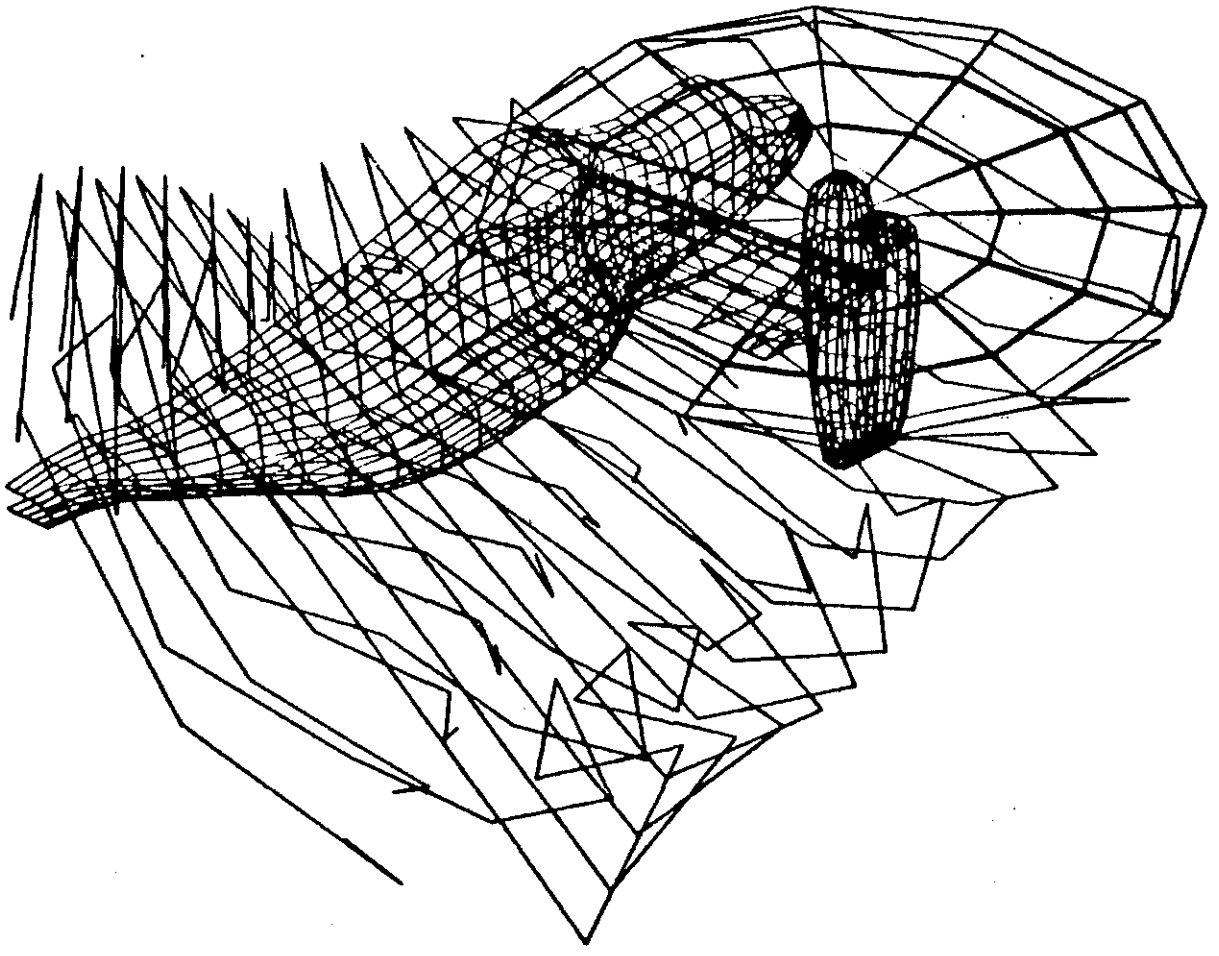

Figure 12(b). Details of the Overall Wake Structure for a Typical Transition Flight Condition; Airspeed 45 Kts, $\alpha = -1.5°$, $C_T = 0.015$

Wing and Rotor Wake Interaction; Wakes Drawn with Cross Elements.

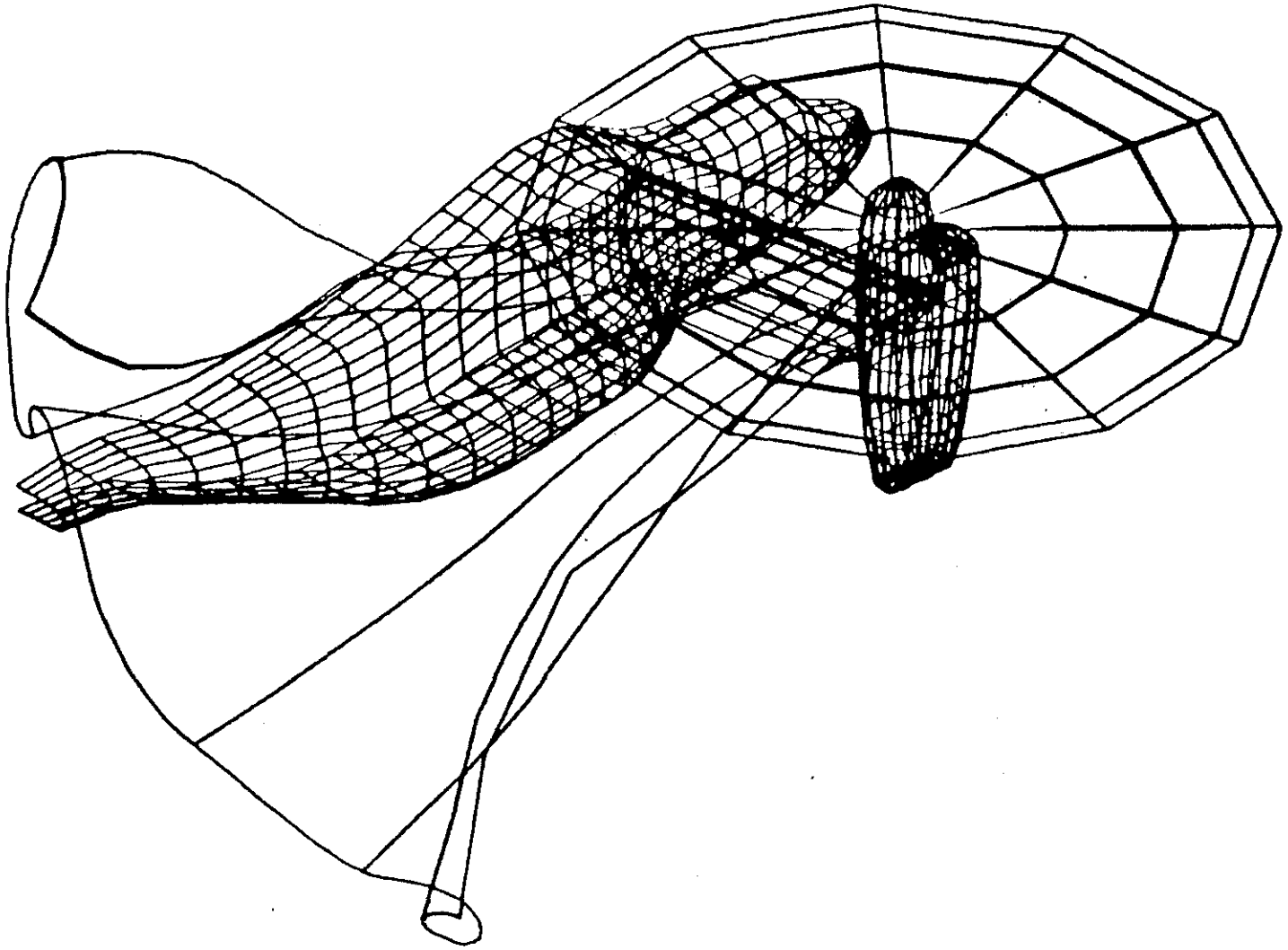

Figure 12(c). Wing Wake Only; Wakes Drawn with Streamwise Filaments

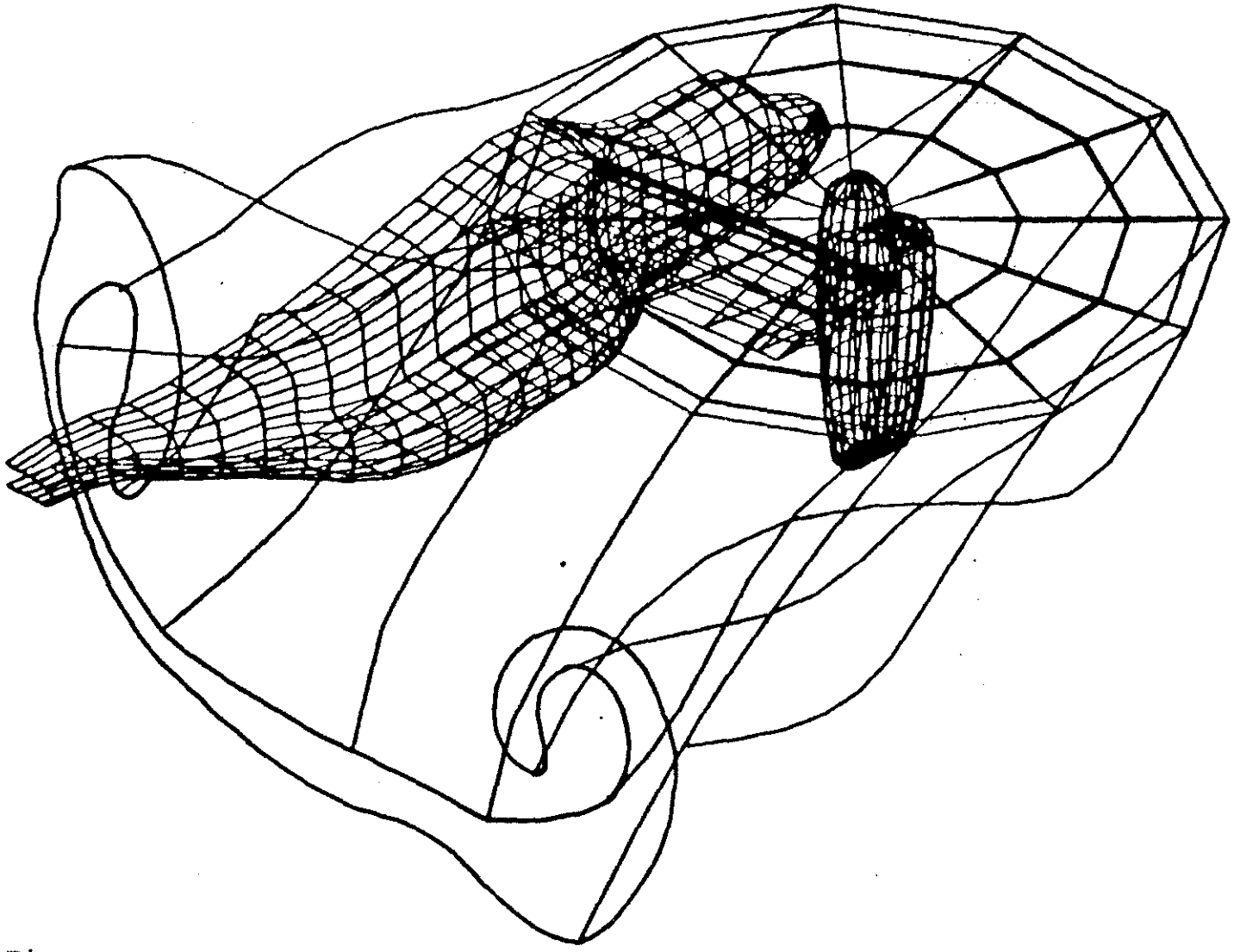

Figure 12(d). Rotor Wake Only; Wakes Drawn with Streamwise Filaments

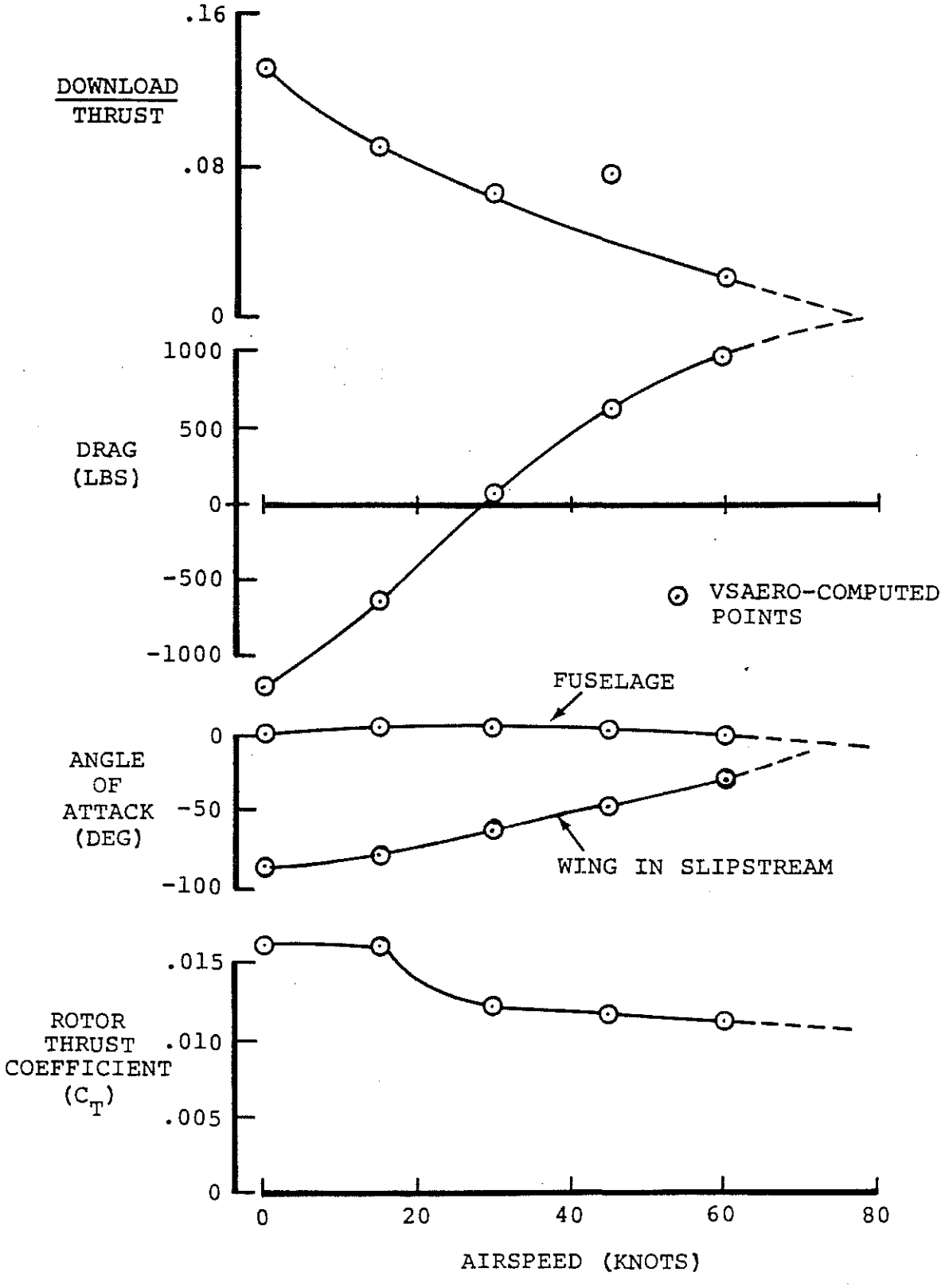

Figure 13. Computed Variation of Download and Drag in Transition: i_p= 90°, Flaps up, Tail off